Discovery of SARS-CoV-2 Inhibitors Featuring Novel Histidine α-Nitrile Motif

A Research work submitted to
Sun Pharma Science Foundation Science Scholar Fellowship – 2024
(Pharmaceutical Sciences)

By

Nilu Vijay Gone

National Chemical Laboratory

Organic Chemistry Division

CSIR-National Chemical Laboratory

Dr. Homi Bhabha Road

Pune-411008, India

E-mail: nv.gone@ncl.res.in

August 2024

1. Introduction

The 'COVID-19 pandemic' has rapidly infected more than half a billion people across the globe, causing unprecedented loss of life and economy, and also becoming one of the biggest public health catastrophes in contemporary times.[1] The infectious agent of COVID-19, severe acute respiratory syndrome coronavirus 2 (SARS-CoV-2), is an enveloped single-stranded RNA virus of the genus *Betacoronavirus* belonging to the *Coronaviridae* family.[2–4] Substantially, a new variant with a detrimental change in the spike would neutralize the vaccine's activity and expose humans to more epidemic threats in the future.[5] SARS-CoV,[6] first reported in 2003, shares 78% genetic similarity with the COVID-19 etiological agent SARS-CoV-2.[7] Owing to the possibility of recurrent mutations evading currently developed vaccines, there is an urgent need to develop effective SARS-CoV-2 antivirals.[8]

1.1 Development of M^{pro} inhibitors to block key steps of the life cycle of SARS-CoV-2

SARS-CoV-2 viral nucleocapsid is endowed with one of the largest genomic RNAs (~30kb).[9] The binding of the spike protein of SARS-CoV-2 virus to ACE2 receptor of host leads to membrane fusion to release of the viral RNA in the cytoplasm of infected cells.[10] The viral RNA translate into two polyproteins (pp1a and pp1ab) which are processed by two viral proteases, PL^{pro} (Papain-like protease) and $3CL^{pro}$ or M^{pro} (Main protease) perform the cleavage activity of polyprotein - a crucial step for the replication of the virus.[11] Among them M^{pro}, a class of highly conserved cysteine proteases found in CoVs that plays an indispensable role in viral replication, is capable of cleaving polyproteins at nearly eleven sites with three times more cleavage affinity compared to PL^{pro} (Fig. 1, *vide infra*).[12] SARS-CoV-2 M^{pro} belongs to the cysteine protease class featuring two protomers which upon dimerization and activation assume appropriate conformation to implement the catalytic functions.[13] Resembling to other cysteine proteases, each protomer is divided into three domains (I, II and III), and its active catalytic dyad is embedded between the cleft of domain II and III of amino acid Cys145 and His41.[14] The thiol group of Cys145 acts as a nucleophile that could attack on electrophilic carbonyl group of amide linkage of substrate polyproteins and the histidine acts as a general base for transfer of proton

generating the acyl-enzyme complex thus resulting in the peptide bond cleavage of polyproteins.[15]

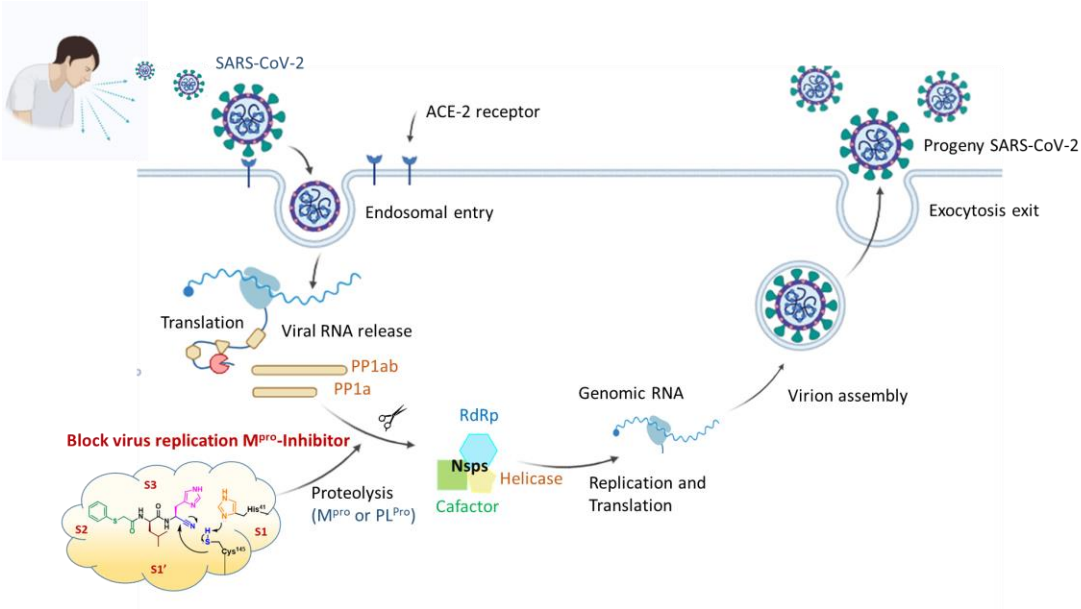

Figure 1. Illustrating the key steps of the life cycle of SARS-CoV-2. Multiple steps in the life cycle of the virus are presented, including the binding of the spike protein to ACE2, endosomal entry of virus into host cell, release of the viral RNA, translation of the viral RNA to polyproteins, proteolysis of polyproteins (pp1ab and pp1a) by main protease (M^{pro}) with papain-like protease (PL^{Pro}), replication and translation to genomic RNA, packaging and assembly of viral particles, and virion release.[12] (Created with BioRender.com)

Accordingly, therapeutics are being developed to block M^{pro} activity during viral genome replication. The electrophilic groups of ligands which can interact with the thiol group of cysteine is commonly referred to as "warhead groups". Several short peptides and peptidomimetics featuring diverse warhead groups have been recently reported as SARS-CoV M^{pro} inhibitors.[16] Various M^{pro} inhibitors have been reported recently to specifically bind covalently to Cys145 with a variety of warhead groups such as: α-ketoamides, α,β-unsaturated ketones, aldehydes, nitrile, etc.[17,18] Structural modification of the potent drug candidate 2 and its related aldehyde 3 led to the discovery of water-soluble prodrug 1 (PF-07304814). Extensive structural modifications on the earlier clinical candidate lufotrelvir further led to the development of nirmatrelvir – a potent antiviral medication developed by Pfizer, which is marketed as Paxlovid – in combination with ritonavir (Fig. 2, *vide infra*).[19,20]

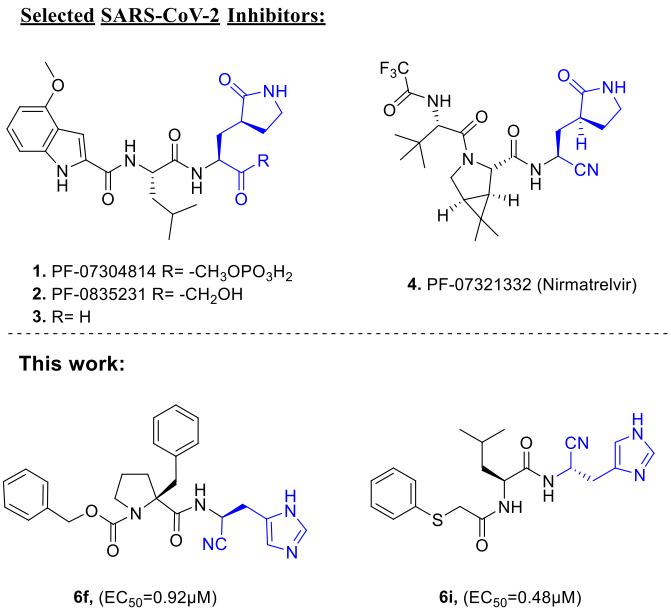

Figure 2. Structures of selected SARS-CoV-2 inhibitors (top) and a short peptide featuring histidine *α*-nitrile **6f** and **6i**, are described in this work.

2. Objectives

As COVID-19 infection caused severe public health concerns recently, the development of novel antivirals has become the need of the hour. This project is therefore aimed at development of a novel class of SARS-CoV-2 main protease (M^{pro}) inhibitor, featuring histidine *α*-nitrile motif embedded on a simple dipeptide framework. SARS coronavirus (CoV) 3CL protease inhibitors featuring cyclic glutamine *γ*-lactam ring *α*-nitrile motif[21] and histidine *α*-aldehyde motif[22] have been reported recently. We envisaged that making a hybrid analog featuring histidine *α*-nitrile motif would enrich the arsenal of warhead groups aimed at targeting SARS coronavirus (CoV) 3CL protease. The histidine *α*-nitrile motif, owing to its electrophilic character, could potentially form a covalent bond with thiol group of Cys145 unit of catalytic dyad (Cys145-His41) present in the active site of the mature dimeric M^{pro} (Fig. 3, *vide infra*). The novel histidine *α*-nitrile motif was planned to be conjugated with various short peptide sequences of hydrophobic nature.

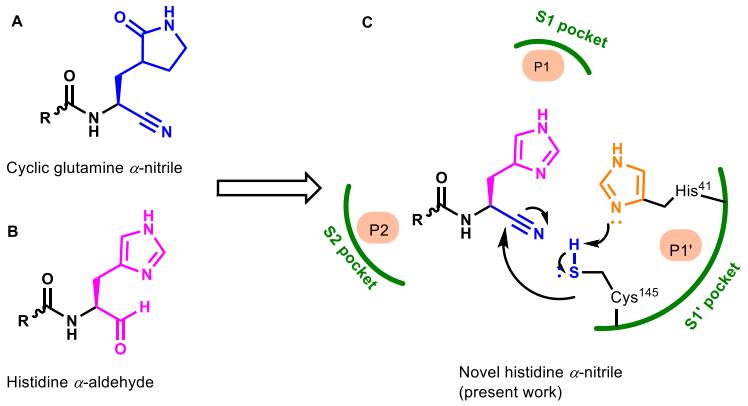

Figure 3. Illustrating the rationale behind designing histidine α-nitrile motif as SARS-CoV-2 M^{pro} inhibitor. Structural motif of glutamine γ-lactam α-nitrile (A), histidine α-aldehyde (B), and designed hybrid structure of histidine α-nitrile motif (C, present work) and its anticipated interaction in binding pockets in the active site of catalytic Cys145-His41 dyad M^{pro}.

Herein, we reported a novel class of short peptides featuring histidine α-nitrile motif and their inhibitory activity against wild-type (WT) SARS-CoV-2.[23] Nine short peptides, carrying histidine α-nitrile motif, were synthesized having diverse structural modifications on the peptide backbone. All peptides were tested for their antiviral potency and comparisons were made of their activity profile with results obtained from *in-silico* studies. *In-vitro* screening suggested that dipeptides featuring this novel histidine α-nitrile motif exhibited antiviral activity and corresponding molecular dynamics simulation studies revealed promising ability to specifically target M^{pro} binding pockets. (Crystal structure PDB ID: 7ALH).

3. Materials and Methods

3.1: Synthesis of histidine α-nitrile dipeptides:

The synthesis of short peptides containing the histidine α-nitrile motif is divided into two schemes (*vide infra*). The initial goal was to synthesize trityl-protected histidine aminonitrile **4** - a common intermediate for compounds **6a-i**. The intermediate **4**[24] was synthesized by using a solution-phase peptide coupling reaction of Fmoc-His-(Trt)-OH with ammonium bicarbonate in the presence of a coupling reagent HBTU/HOBt and DIPEA in DMF to obtain the amide **2** in good yield**.** The preparation of Fmoc-His-(Trt)-α-nitrile **3** from amide **2** was achieved by its dehydration

using *in-situ* generated Vilsmeier–Haack reagent. Fmoc deprotection of **3** was achieved by a 50% mixture of *tert*-butylamine in dichloromethane to obtain the intermediate **4** in good yield**.**

3.2 Scheme I. Synthesis of trityl-protected histidine aminonitrile **4**.

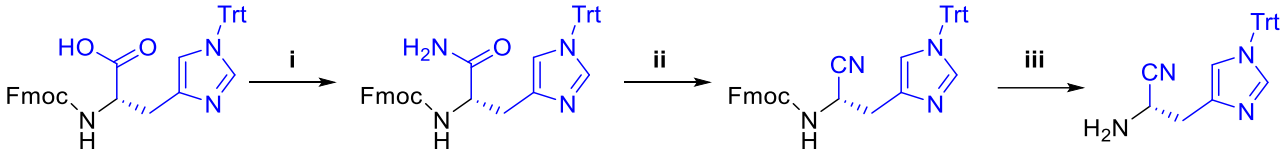

1 **2,** 86% **3,** 74% **4,** 70%

Reaction conditions: (i) Ammonium bicarbonate, HBTU, HOBt, DIPEA, dry DMF, 0 °C - rt, 10 h; (ii) $(COCl)_2$, triethylamine, dry DMF, dry ACN, 0 °C - rt, 1 h; (iii) *tert*-butylamine:DCM (1:1), rt, 30 min.

3.3 Scheme II. Synthesis of trityl-deprotected histidine *α*-nitrile dipeptides **6a-i**.

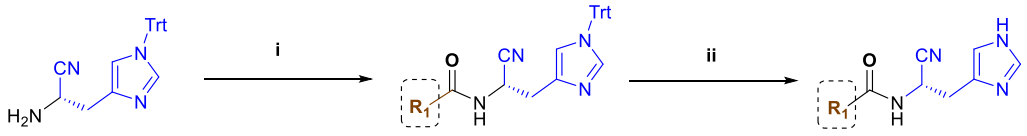

4 **5a-i** (62-77%) **6a-i** (55-68%)

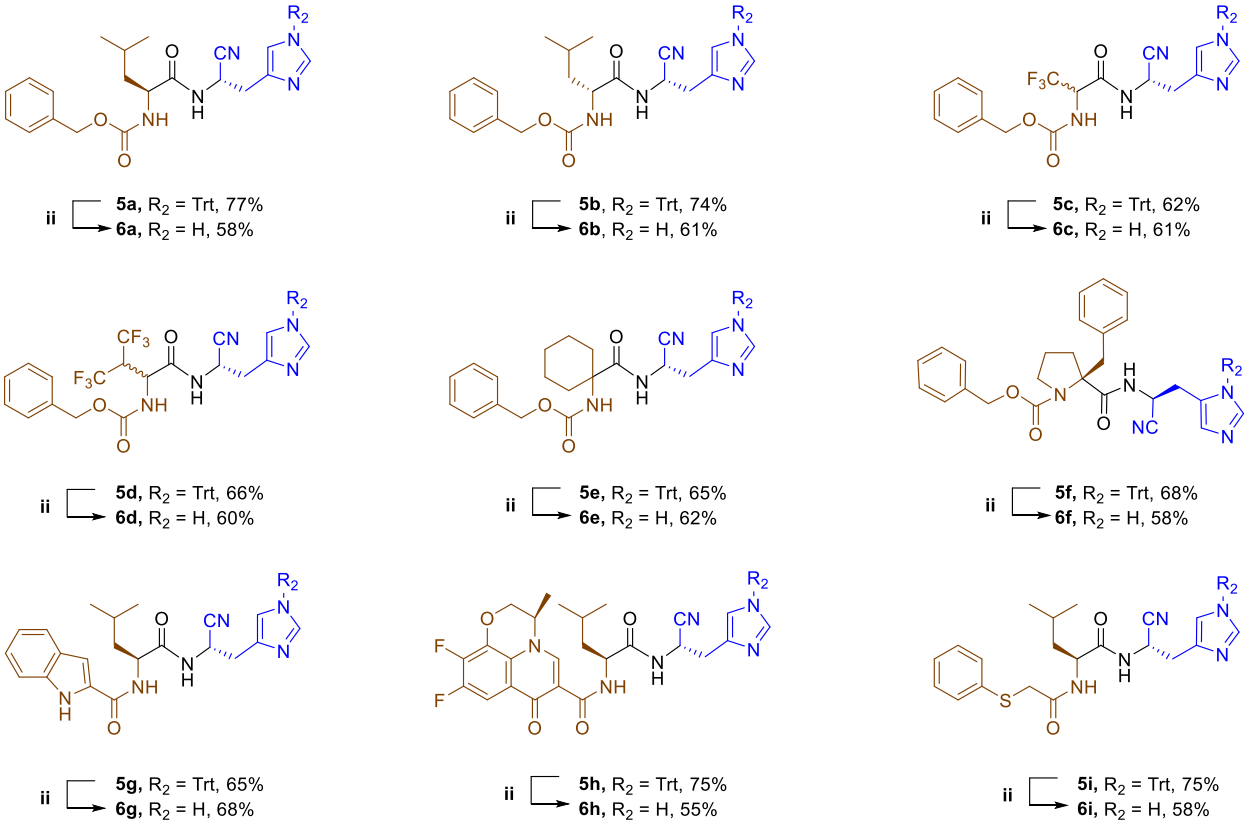

ii → **5a,** R_2 = Trt, 77%; **6a,** R_2 = H, 58%

ii → **5b**, R_2 = Trt, 74%; **6b**, R_2 = H, 61%

ii → **5c,** R_2 = Trt, 62%; **6c,** R_2 = H, 61%

ii → **5d,** R_2 = Trt, 66%; **6d,** R_2 = H, 60%

ii → **5e,** R_2 = Trt, 65%; **6e,** R_2 = H, 62%

ii → **5f,** R_2 = Trt, 68%; **6f,** R_2 = H, 58%

ii → **5g,** R_2 = Trt, 65%; **6g,** R_2 = H, 68%

ii → **5h,** R_2 = Trt, 75%; **6h,** R_2 = H, 55%

ii → **5i,** R_2 = Trt, 75%; **6i,** R_2 = H, 58%

Reaction conditions: (i) R_1-COOH, HBTU, HOBt, DIPEA, DMF, 0 °C - rt, 16 h; (ii) 60% TFA in DCM, 0 °C - rt, 45 min.

Scheme II (*vide supra*) illustrates the coupling reaction of intermediate **4** with different carboxylic acids in the presence of HBTU/HOBt and DIPEA in DMF to furnish trityl-protected dipeptides **5a-i**, which upon removal of the trityl-protecting group with 60% TFA in DCM afforded **6a-i** in good yields.

4. Results, Statistical Analysis, Discussion

4.1 Structure-activity relationship of histidine *α*-nitrile dipeptides 6a-i

Preliminary screening was performed using infected Vero (African green monkey kidney cells, Vero (ATCC® CCL-81™) cells with SARS-CoV-2 virus (A3i clade), which were treated with a series of nine compounds and RT-qPCR assays were performed to determine the percentage of viral growth reduction using different concentrations. The assay results showed that the new series of histidine *α*-nitrile dipeptides **6a-i** is effective for growth suppression of SARS-CoV-2 at low micro-molar concentrations, except for the compounds **6a, 6e** and **6h** (Fig. 4, *vide infra*). We synthesized histidine *α*-nitrile dipeptides **6a-i** containing nitrile warhead with variable Leucine and Cbz group's substitutions. The dipeptide **6a** showed no considerable viral reduction (Fig. 4a, *vide infra*); thus, it can be speculated to serve as a platform for the optimized synthesis of potent molecules that bind to the M^{pro} target. Compound **6b** exhibited a stagnant profile of a 45%-48% increase in viral growth suppression at concentrations between ≃5 μM-25 μM (desired regime limit of Fig. 4b, *vide infra*), which was caused by a change in the stereochemical configuration of Leucine in compound **6a**. Thus, consequent studies were conducted to modify structure **6a** to enhance its potency.

Furthermore, compound **6c** is significantly more potent than compound **6a**, as it exhibited a lead-in suppression value of 47% at 1 μM. We observed a hike in viral growth suppression with the increase in the concentration (Fig. 4c, *vide infra*), indicating that introducing the trifluoro may also play a significant role in inhibition activity. The trifluoro group is partially solvent-exposed, and through this interaction, it penetrates the S1 pocket with an additional hydrogen bond with Glu166 in a catalytic pocket (Fig. 7a2, *vide infra*). In **6d**, the hexafluoro-valine linked with the histidine *α*-nitrile motif has substantially more activity than **6a** but less in comparison to **6c**.

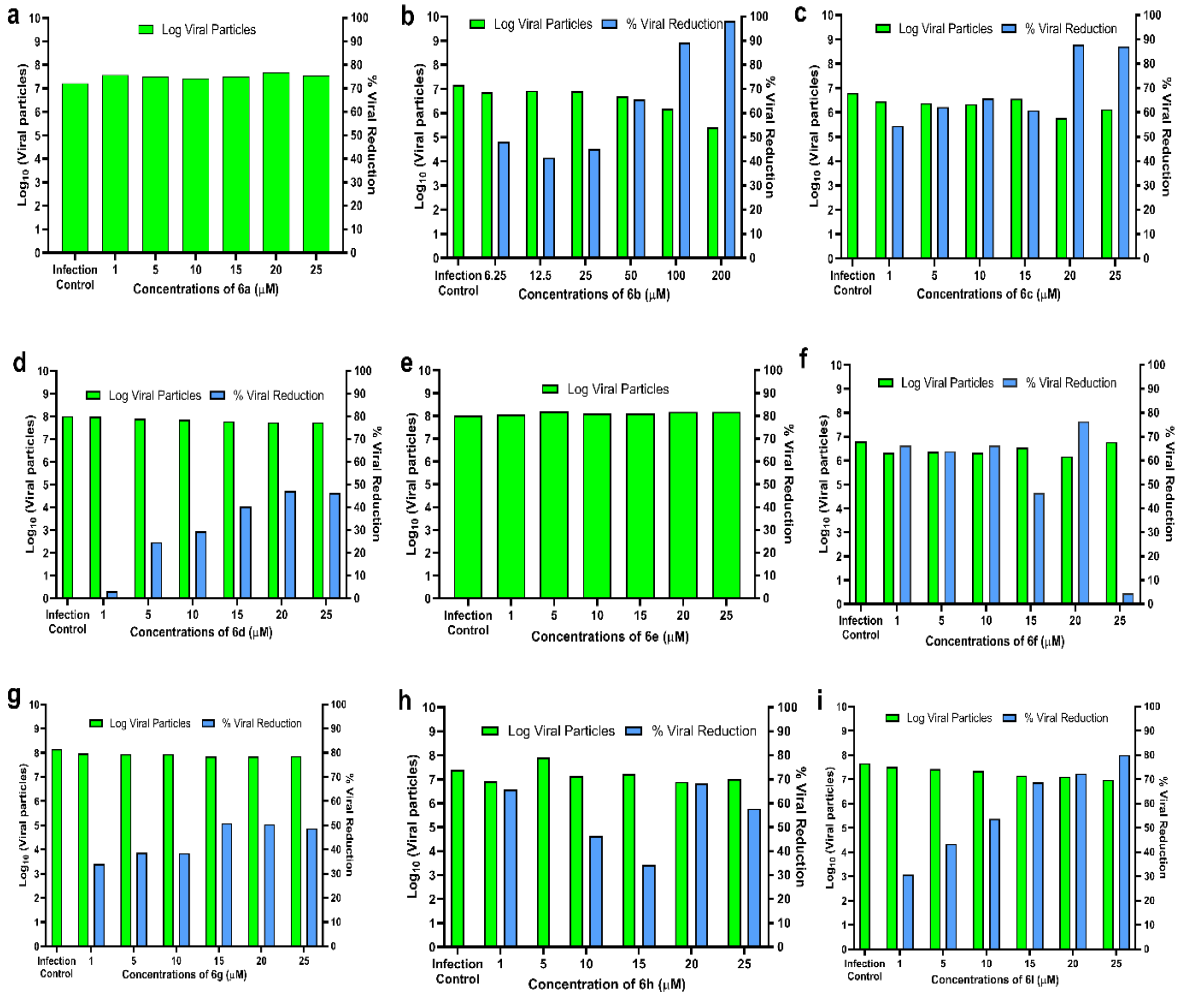

Figure. 4. Preliminary antiviral activity of histidine α-nitrile dipeptides **6a-i** in Vero cells infected with SARS-CoV-2.

Notably, compound **6e** from this series was inactive against SARS-CoV-2, which might be due to the presence of a cyclic system and the lack of stereochemistry in place of Leucine. Relatively, the replacement of Leucine to (S)-2-benzyl proline in compound **6f** did reveal potent behavior from the base concentration. Its activity profile is also marginally similar to compound **6c**. We understand that the presence of the 2-benzyl proline amino acid in **6f** invigorates itself to its structural counterpart **6e**. To continue our SAR studies on **6a**-**f** molecules, we synthesized another set of compounds that replace the Cbz-group. Previous studies indicated that the Leucine amino acid scaffolds possibly inhibited COVID-19 virus infection in Vero cells through hydrophobic nonbonding interactions within the enzyme's catalytic pocket. We synthesized the compounds with modification on **6a,** increasing the growth suppression activity, assuming *via* the

desirable protease inhibition, such as compound **6i**. Compound **6g** is structurally mimic to compound **6a** but displayed lower activity than its counterparts **6i** (Fig. 4, *vide supra*).

Further, by increasing the aromatic bulk, we found that the activity varied. For example, a synergistic drug-peptide conjugate, **6h**, containing a molecule of the ofloxacin drug family. When we incorporated that analogous drug entity in the place of the Cbz group, **6h** exhibited an unanticipated therapeutic profile. The compound **6i** being highly efficacious on par with **6c**, stands amidst the series of candidates, exhibiting a favorable profile of viral growth suppression (Fig. 4i, *vide supra*). The thorough evaluation of the efficacies of our candidates of interest (COI) is defined in the results of the 'Anti-COVID activity of selected inhibitors' section. In consensus, the preliminary results concluded that 5 COIs had capable antiviral anticipations - **6c, 6i, 6f, 6d** and **6g** (*named in descending order of profile activity from left to right).* Furthermore, cell viability assays MTT (Fig. 5, *vide infra*), Efficacy experiments (Fig. 6, *vide infra*) and Molecular Dynamics (Fig. 7, *vide infra*), of the finalized compounds were performed to conclude their *in-vitro* anti-COVID potential. We observed that the significant COIs exhibited viral growth inhibition in the micromolar range of potency (EC_{50} from 0.5 µM-1 µM).

4.2 Cytotoxicity Assay

The results obtained from the MTT assay showed that the candidate molecules **6c** (Fig. 5a), **6f** (Fig. 5b) and **6i** (Fig. 5c) did not elicit cytotoxicity and the cell viability ranged ~80 to 90% until 25 µM concentration suggesting that the CC_{50} value is more than 25 µM (Fig. 5, *vide infra*).

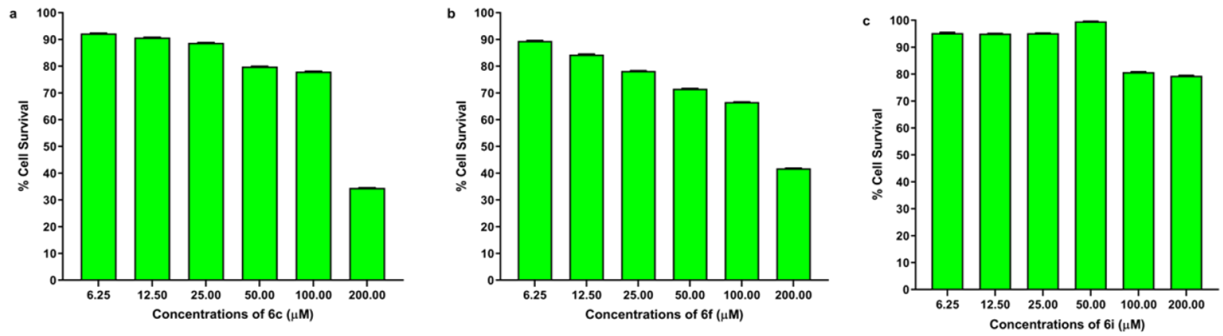

Figure 4. Cell Cytotoxicity of the inhibitor molecule (**6c**, **6f** and **6i**): Vero cells were treated with different concentrations (6.25, 12.5, 25, 50, 100 and 200 µM) of inhibitor molecules. Figure a, b and c represent the percentage of cell viability against concentrations of **6c**, **6f** and **6i,** respectively. The data was analyzed using GraphPad Prism, version 8.4.2 (n=4).

Anti-COVID activity of selected inhibitors (6c, 6f and 6i): The candidate inhibitor molecules showed a considerable reduction in the viral load evidenced through RT-qPCR using SARS-CoV-2 specific primers. The viral particles were enumerated and the Effective Concentration-50 (EC_{50}) for the inhibitors was calculated through 'Dose-response-Stimulation' analysis (Fig. 6, *vide infra*).

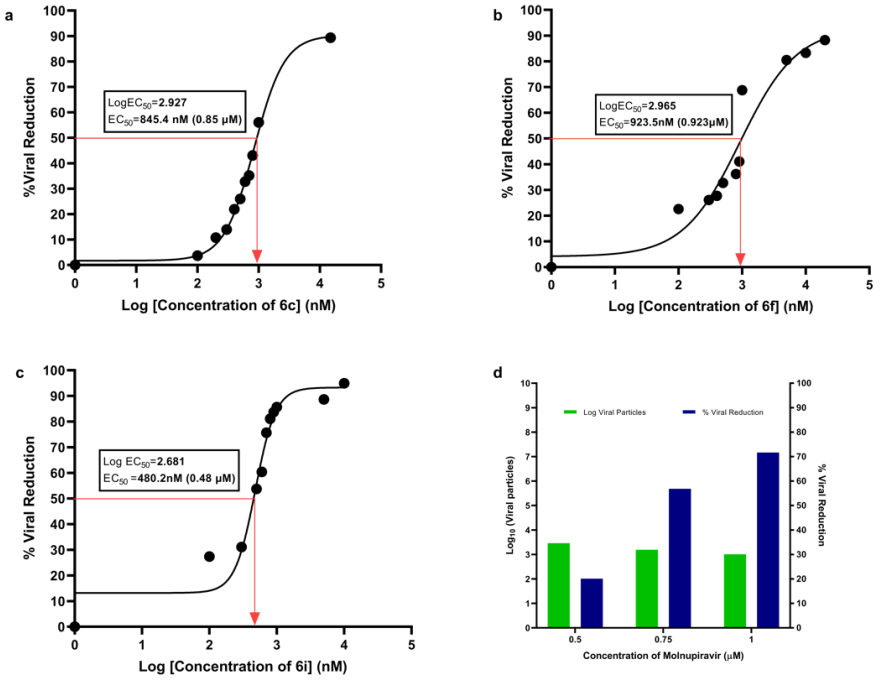

Figure 6. Anti-COVID activity of inhibitor molecules (6c, 6f and 6i): The graph represents the percentage of viral reduction *vs* different concentrations (0.1, 0.2, 0.3, 0.4, 0.5, 0.6, 0.7, 0.8, 0.9, 1, 5, 10, 15, 20 µM) of inhibitor molecules. The viral particles were enumerated by considering SARS-CoV-2 N-gene amplification using RT-qPCR. Figure 5a represents the Log EC_{50} of inhibitor (**6c**) as 2.927, which corresponds to 0.85 µM. Figure 5b represents the Log EC_{50} of inhibitor (**6f**) as 2.965 which corresponds to 0.92 µM, figure 5c the Log EC_{50} of inhibitor (**6i**) as 2.681 which corresponds to 0.48 µM and figure 5d represents the percentage of viral reduction treated with different concentration of Molnupiravir (0.5 µM, 0.75 µM and 1 µM) (n=6).

4.3 Computational Studies

M^{pro}–inhibitors binding interactions

Based on their bioactivity profiles, interactions of the three most potent inhibitors (**6c**, **6f** and **6i**) with M^{pro} are investigated by combining molecular docking and molecular dynamics (MD) simulations. The binding cavity of M^{pro} includes four sites, namely S1, S1', S2 and S3, for these

inhibitors. The MD equilibrated structure of the **6c**-M^{pro} complex shows that the binding of **6c** encompasses the S1 and S2 binding sites (Fig. 7a1, *vide infra*). In this binding mode, the imidazole group containing moiety of **6c** is stabilized by a hydrogen bond with His163 in the S1 site, while its phenyl group is located in the S2 site adjacent to Met49 (Fig. 7a2, *vide infra*). The amide group of this inhibitor forms a hydrogen bond with the backbone of Glu166 in the S1 pocket, and the remaining trifluoro substituent is partially solvent-exposed. Due to these interactions, **6c** penetrates deeply into the S1 region of M^{pro}. It can potentially form another hydrogen bond with the adjacent Glu166, upon the covalent binding of the nitrile warhead of **6c** to Cys145. The binding energy of **6c** computed using the Molecular Mechanics – Poisson Boltzmann Surface Area (MM-PBSA) method is -28.7± 5.1 Kcal/mol.

On the other hand, the **6f** inhibitor predominantly binds through hydrophobic interactions in the S1' and S2 binding sites of M^{pro} (Fig. 7b1, *vide infra*). In particular, its phenyl groups effectively occupy the S2 hydrophobic pocket surrounded by Met49 and His41 (Fig. 7b2, *vide infra*). In this mode, the sterically hindered azolidine ring is buried into the S3 site (Fig. 7b1, *vide infra*). It is further stabilized by the formation of a hydrogen bond with His41 located at the intersection of the S1' and S2 binding sites. These interactions position the nitrile warhead of **6f** close to Cys145. This inhibitor's binding energy of -34.9 ± 2.7 Kcal/mol is approximately 6.0 Kcal/mol higher than the one computed for **6c**. The **6i** inhibitor binds in the S1, S1', and S2 binding sites of M^{pro} (Fig. 7c1, *vide infra*). Its imidazole group is positioned in the S1 site, while the Cbz group is positioned in the S2 binding site (Fig. 7c1, *vide infra*). In contrast to **6c** and **6f**, it interacts with the binding cavity predominantly through hydrogen bonding. For instance, it forms a hydrogen bond with Cys145 and His41 in the S1' site (Fig. 7c2, *vide infra*). Additionally, the *β*-imidazole group forms a hydrogen bond with the previously inaccessible side chain of Glu166 and positions itself in the proximity of Cys145 in the S1' binding site. Furthermore, the tertiary butyl group of the **6i** inhibitor is found to access the Thr25-Leu27 segment of the S1' binding site. The binding energy of -34.2 ± 7.1 Kcal/mol for **6i** is comparable to the calculated binding free energy for **6f**. The **6i** inhibitor was also docked to another crystal structure (PDB ID: 6LU7). It binds in the same region of the protein with a high docking score of -13.9 (Fig. 8, *vide infra*). Notably, these binding modes are similar to those proposed in a previous study using a different peptidomimetic inhibitor.[25]

These results suggest that the imidazole group of histidine α-nitrile motifs preferably binds in the S1 pocket, while the Cbz terminal is in the S2. The central fragment usually occupies either the S1' binding site or is exposed to solvent. Although all of them bind in distinct modes to $M^{pro,}$ they position the critical nitrile warhead in the vicinity of Cys145.

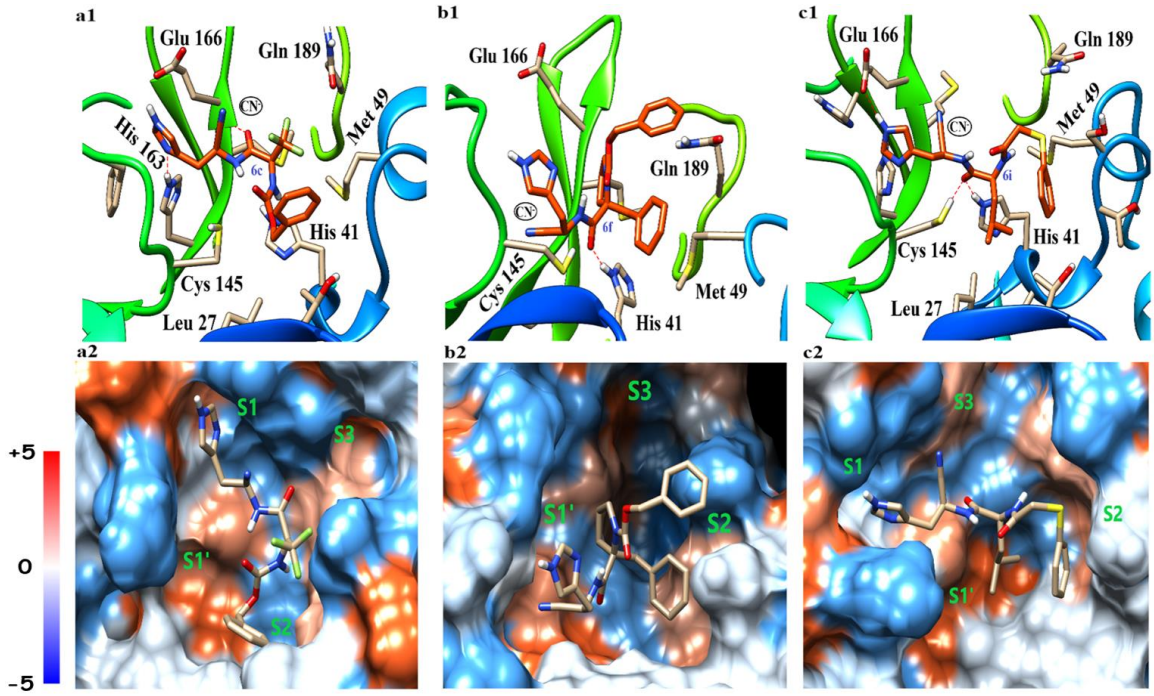

Figure 7. Binding modes of M^{pro}-inhibitor complex: Electrostatic potential surface and non-covalent interactions of the Main protease (SARS-CoV-2) with **6c** (a1 and a2), **6f** (b1 and b2) and **6i** (c1 and c2) inhibitors. Surface assigned according to Kyle-Doolittle Scale with positive values depicting hydrophobic nature.[26]

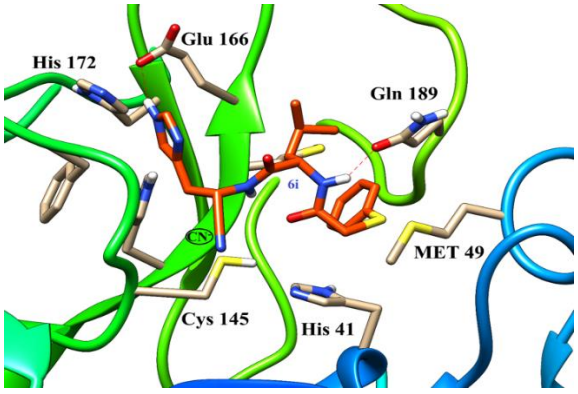

Figure 8. Docking pose of **6i** in complexation with M^{pro} (PDB ID: 6LU7). The binding energy and score from the docking procedure are -7.9 kcal/mol and -13.96, respectively. The inhibitor forms hydrogen bonds with Glu166 and Gln189, with the imidazole ring positioned into the S1 subsite and the Cbz group occupying the S2/S3 subsite. The α-nitrile warhead is positioned close to Cys145.

Antiviral studies and molecular docking analysis suggested that the compounds **6c**, **6f**, and **6i** showed the strong binding activity in a substrate-like fashion, which may lead to competitive inhibition of their activity. The CC_{50} value, EC_{50} value, docking score, binding energy and docking pose suggests that all three molecules showed significant binding with SARS-CoV-2 M^{pro} (Table 1, *vide infra*). Furthermore, the binding energies of the inhibitors were computed using the Molecular Mechanics – Poisson Boltzmann Surface Area (MM-PBSA) method[27] the root-mean-square deviation (RMSD) of these simulations showed that they were well equilibrated within the time frame of simulations (Fig. 9, *vide infra*).

Table 1: *In-vitro* and *in-silico* screening of potent histidine *α*-nitrile dipeptides

	In-vitro		***In-silico***		
Compound No.	Cell cytotoxicity CC_{50} (μM)	Effective concentration EC_{50} (μM)	Docking score (Kcal/mol)	Binding energy (Kcal/mol)	M^{pro} pocket occupation in MD equilibrated structures
6c	>25	0.85	-10.663	-28.7 ± 5.1	S1 and S2
6f	>25	0.92	-13.447	-34.9 ± 2.7	S1'-S3
6i	>25	0.48	-13.924	-34.2 ± 7.1	S1-S2

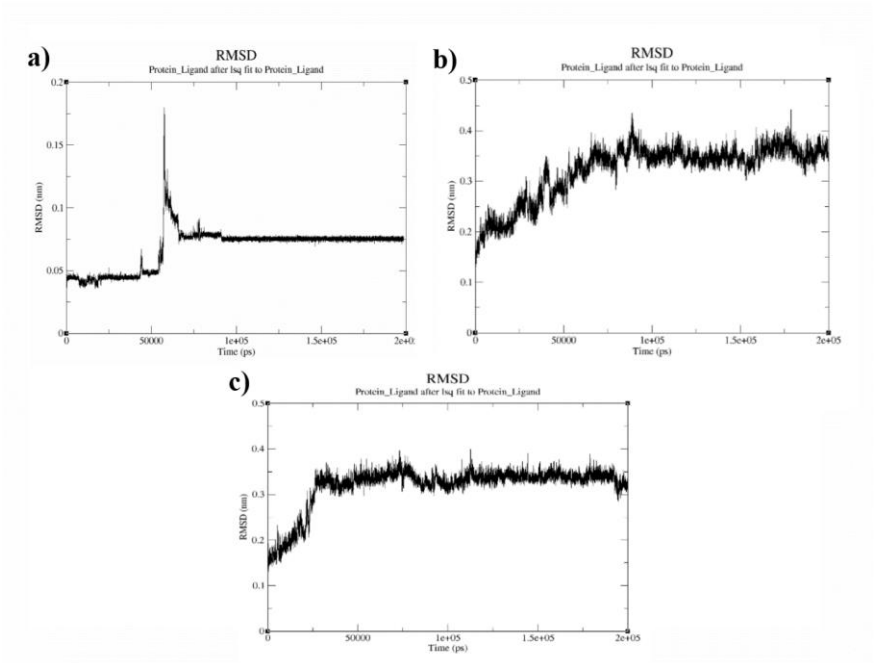

Figure 9. RMSD plots of the protein-inhibitor complexes. (a) M^{pro}-**6c**, (b) M^{pro}-**6f** and (c) M^{pro}-**6i**.

In silico ADME studies

Absorption, distribution, metabolism, and excretion (ADME) parameters of these ligands were predicted by the Swiss ADME server, depicted in Table 2 (Fig. 10).[28]

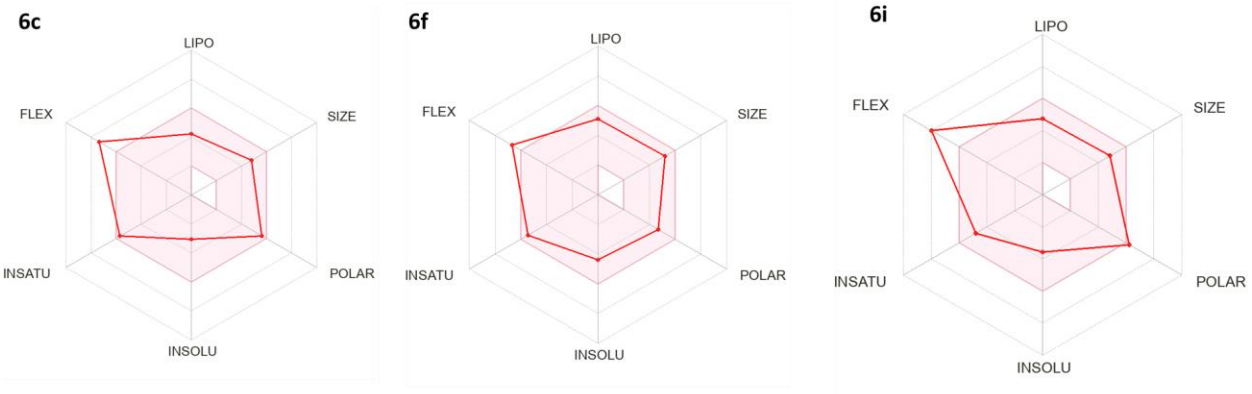

Figure 10: The oral bioavailability radar of compounds **6c**, **6f** and **6i** using the Swiss ADME predictor. The six physiochemical properties consider to qualify a molecules as drug-like are lipophilicity (LIPO), size (SIZE), polarity (POLAR) and solubility (INSOLU), saturation (INSATU) and flexibility (FLEX).

Table 2: In silico, ADME parameters for ligands predicted through the Swiss ADME server

Compound No.	Mwt	GI absorption	Drug likeliness					BA Score
			Lipinski violations	Ghose Violations	Veber Violations	Egan violations	Muegge violations	
6c	399.51	High	0	0	1	1	0	0.55
6f	429.51	High	0	0	0	0	0	0.55
6i	395.34	High	0	0	1	0	0	0.55

5. Conclusion

The contagious epidemic threat of COVID-19 disease, caused by the SARS-CoV-2 virus and its mutated variants, wreaked havoc globally, challenging the vaccine's potential efficacy. One of the strategies to combat the pandemic is to develop a potent antiviral agent that inhibits the replication pathway of the SARS-CoV-2 virus. The M^{pro} is a fundamental enzyme for viral protein synthesis, which is required for viral replication and maturation. The development of potent M^{pro} inhibitors is thus one of the key strategies to develop potent drug molecules to fight the dreaded SARS-CoV-2. This study describes the design and synthesis of histidine α-nitrile motif embedded in a simple dipeptide backbone and the inhibitory activity of these compounds against the SARS-

CoV-2 M^{pro}. The *in-vitro* testing of the selected inhibitors (**6c**, **6f** and **6i**) with histidine α-nitrile motif showed potential anti SARS-CoV-2 activity. *In-silico* studies suggest that the nitrile group of the histidine α-nitrile motif can interact with the nucleophilic thiol group of Cys145 residue of the protease, resulting in the formation of a reversible covalent thioimidate adduct in the active catalytic site of the S1' pocket (Fig. 7, vide supra). They may lead to the design of the next generation of molecules for the therapeutic prevention of SARS-CoV-2. Overall, our findings suggest that structurally modest short peptides featuring histidine α-nitrile motifs may offer utility in the development of effective therapeutics as M^{pro} inhibitors.

6. Impact of the research in the advancement of knowledge or benefit to mankind

Our reported histidine α-nitrile motif, a novel class of SARS-CoV-2 main protease (M^{pro}) inhibitor, would be potent drug candidate to fight the dreaded SARS-CoV-2 and its variants. Indeed, the simple dipeptide structural framework, amenable to quick structural variations, coupled with ease of synthesis from readily available commercial starting materials are the major attractive features of this novel class of SARS-CoV-2 inhibitors. The practical utility of histidine α-nitrile dipeptides would have beneficial impact during such pandemic in future with lower risk of life and economy.

7. Literature reference

[1] "WHO Coronavirus (COVID-19) Dashboard | WHO Coronavirus (COVID-19) Dashboard with Vaccination Data," can be found under https://covid19.who.int/.

[2] N. M. Anand, D. H. Liya, A. K. Pradhan, N. Tayal, A. Bansal, S. Donakonda, A. K. Jainarayanan, *PLoS. One.* **2021**, *16*, 1-21.

[3] L. Zhang, D. Lin, X. Sun, U. Curth, C. Drosten, L. Sauerhering, S. Becker, K. Rox, R. Hilgenfeld, *Science* **2020**, *368*, 409-412.

[4] C. S. Dampalla, Y. Kim, N. Bickmeier, A. D. Rathnayake, H. N. Nguyen, J. Zheng, M. M. Kashipathy, M. A. Baird, K. P. Battaile, S. Lovell, S. Perlman, K. O. Chang, W. C. Groutas, *J. Med. Chem.* **2021**, *64*, 10047-10058.

[5] X. R. Ma, Y. R. Alugubelli, Y. Ma, E. C. Vatansever, D. A. Scott, Y. Qiao, G. Yu, S. Xu, W. R. Liu, *Chem. Med. Chem.* **2022,** *17*, 1-8.

[6] M. D. Sacco, C. Ma, P. Lagarias, A. Gao, J. A. Townsend, X. Meng, P. Dube, X. Zhang, Y. Hu, N. Kitamura, B. Hurst, B. Tarbet, M. T. Marty, A. Kolocouris, Y. Xiang, Y. Chen, J. Wang, *Sci. Adv.* **2020**, *6*, 1-15.

[7] T. Pillaiyar, M. Manickam, V. Namasivayam, Y. Hayashi, S. H. Jung, *J. Med. Chem.* **2016**, *59*, 6595-6628.

[8] D. Bojadzic, O. Alcazar, J. Chen, S. T. Chuang, J. M. C. Capcha, L. A. Shehadeh, P. Buchwald, *ACS Infect. Dis.* **2021**, *7*, 1519-1534.

[9] T. Muramatsu, C. Takemoto, Y. T. Kim, H. Wang, W. Nishii, T. Terada, M. Shirouzu, S. Yokoyama, *Proc. Natl. Acad. Sci. U. S. A.* **2016**, *113*, 12997-13002.

[10] A. D. Rathnayake, J. Zheng, Y. Kim, K. Dinali Perera, S. Mackin, D. K. Meyerholz, M. M. Kashipathy, K. P. Battaile, S. Lovell, S. Perlman, W. C. Groutas, K. O. Chang, *Sci. Transl. Med.* **2020***, 12,* 1-11*.*

[11] Y. Liu, C. Liang, L. Xin, X. Ren, L. Tian, X. Ju, H. Li, Y. Wang, Q. Zhao, H. Liu, W. Cao, X. Xie, D. Zhang, Y. Wang, Y. Jian, *Eur. J. Med. Chem.* **2020**, *206*, 112711.

[12] W. Dai, B. Zhang, X. M. Jiang, H. Su, J. Li, Y. Zhao, X. Xie, Z. Jin, J. Peng, F. Liu, C. Li, Y. Li, F. Bai, H. Wang, X. Cheng, X. Cen, S. Hu, X. Yang, J. Wang, X. Liu, G. Xiao, H. Jiang, Z. Rao, L. K. Zhang, Y. Xu, H. Yang, H. Liu, *Science* **2020**, *368*, 1331-1335.

[13] A. Citarella, A. Scala, A. Piperno, N. Micale, *Biomolecules* **2021**, *11*, 607.

[14] J. Qiao, Y. S. Li, R. Zeng, F. L. Liu, R. H. Luo, C. Huang, Y. F. Wang, J. Zhang, B. Quan, C. Shen, X. Mao, X. Liu, W. Sun, W. Yang, X. Ni, K. Wang, L. Xu, Z. L. Duan, Q. C. Zou, H. L. Zhang, W. Qu, Y. H. P. Long, M. H. Li, R. C. Yang, X. Liu, J. You, Y. Zhou, R. Yao, W. P. Li, J. M. Liu, P. Chen, Y. Liu, G. F. Lin, X. Yang, J. Zou, L. Li, Y. Hu, G. W. Lu, W. M. Li, Y. Q. Wei, Y. T. Zheng, J. Lei, S. Yang, *Science* **2021**, *371*, 1374-1378.

[15] G. L. Monica, A. Bono, A. Lauria, A. Martorana, *J. Med. Chem.* **2022**, *65*, 12500-12534.

[16] Several short hydrophobic peptides featuring diverse war head groups targeting $3CL^{pro}$ and PL^{pro} of SARS-CoV-2 have been reported recently. Z. Xia, M. Sacco, Y. Hu, C. Ma, X. Meng, F. Zhang, T. Szeto, Y. Xiang, Y. Chen, J. Wang, *ACS Pharmacol. Transl. Sci.* **2021**, *4*, 1408-1421.

[17] C. P. Chuck, C. Chen, Z. Ke, D. C. C. Wan, H. F. Chow, K. B. Wong, *Eur. J. Med. Chem.* **2013**, *59*, 1-6.

[18] R. L. Hoffman, R. S. Kania, M. A. Brothers, J. F. Davies, R. A. Ferre, K. S. Gajiwala, M. He, R. J. Hogan, K. Kozminski, L. Y. Li, J. W. Lockner, J. Lou, M. T. Marra, L. J. Mitchell, B. W. Murray, J. A. Nieman, S. Noell, S. P. Planken, T. Rowe, K. Ryan, G. J. Smith, J. E. Solowiej, C. M. Steppan, B. Taggart, *J. Med. Chem.* **2020**, *63*, 12725-12747.

[19] D. Y. Duveau, C. J. Thomas, *ACS Pharmacol. Transl. Sci.* **2022**, *5*, 445-447.

[20] L. Vangeel, W. Chiu, S. D. Jonghe, P. Maes, B. Slechten, J. Raymenants, E. André, P. Leyssen, J. Neyts, D. Jochmans, *Antiviral Res.* **2022**, *198*, 105252.

[21] Faridoor, R. Ng, G. Zhang, J. J. Li, *Med. Chem. Res.* **2023**, *32*, 1039-1062.

[22] K. Akaji, H. Konno, H. Mitsui, K. Teruya, Y. Shimamoto, Y. Hattori, T. Ozaki, M. Kusunoki, A. Sanjoh, *J. Med. Chem.* **2011**, *54*, 7962-7973.

[23] While this work was in progress, we came across a patent reporting histidine alpha nitrile motif. L. D. Arnold, A. Jennings, W. Keung. Pardes Biosciences, Inc., inhibitors of cysteine proteases and methods of use thereof. United States Patent US 11,124,497 Bl. **2021** Sep 21.

[24] S. Mondal, Y. Chen, G. J. Lockbaum, S. Sen, S. Chaudhuri, A. C. Reyes, J. M. Lee, A. N. Kaur, N. Sultana, M. D. Cameron, S. A. Shaffer, C. A. Schiffer, K. A. Fitzgerald, P. R. Thompson, *J. Am. Chem. Soc.* **2022**, *144*, 21035-21045.

[25] J. Breidenbach, C. Lemke, T. Pillaiyar, L. Schäkel, G. A. Hamwi, M. Diett, R. Gedschold, N. Geiger, V. Lopez, S. Mirza, V. Namasivayam, A. C. Schiedel, K. Sylvester, D. Thimm, C. Vielmuth, L. P. Vu, M. Zyulina, J. Bodem, M. Gütschow, C. E. Müller, *Angew. Chem. Int. Ed.* **2021**, *60*, 10423-10429.

[26] J. Kyte, R. F. Doolittle. *J. Mol. Biol.* **1982**, *157*, 105-32.

[27] M. S. Valdés-Tresanco, M. E. Valdés-Tresanco, P. A. Valiente, E. Moreno, *J. Chem. Theory Comput.* **2021**, *17*, 6281-6291.

[28] A. Daina, O. Michielin, V. Zoete, *Sci Rep.* **2017**, *3*, 7, 42717.

Note: I declare that the research work submitted for Sun Pharma Science Foundation Science Scholar Fellowship Award - 2024 (pharmaceutical sciences) is true and correct to the best of our knowledge.

Applicant Signature:
Name: **Nilu Vijay Gone**
Date: 27th August 2024